INSTITUTE OF PHYSICS PUBLISHING METROLOGIA
Metrologia **43** (2006) 573–582 doi:10.1088/0026-1394/43/6/013

Characterization of a compact 200 MPa controlled clearance piston gauge as a primary pressure standard using the Heydemann and Welch method

A K Bandyopadhyay[1] **and Douglas A Olson**[2]

[1] National Physical Laboratory, Dr K S Krishnan Marg, New Delhi 110012, India
[2] National Institute of Standards and Technology (NIST), 100 Bureau Drive, Gaithersburg, MD 20899-8364, USA

E-mail: akband@mail.nplindia.ernet.in and douglas.olson@nist.gov

Received 9 May 2006
Published 30 November 2006
Online at stacks.iop.org/Met/43/573

Abstract
Controlled clearance piston gauges are used as primary pressure standards at many national metrology institutes. The National Institute of Standards and Technology, in collaboration with the National Physical Laboratory (India), is studying the performance of a new generation of controlled clearance gauges that offer the potential for reduced uncertainties. The gauges are also well suited to interlaboratory comparisons because of their smaller, integrated design and use of existing mass sets. In this paper we present results of the characterization of a 200 MPa oil-operated controlled clearance gauge with a 2.5 mm nominal diameter piston and cylinder. The gauge is operated with an external cylinder pressure of 0 MPa to 80 MPa. We present results of piston fall rate measurements, deformation measurements, piston diameter measurements and modelling calculations using the Heydemann–Welch (HW) method on two occasions over a two-year time period. The relative standard uncertainties in the effective area (A_e) using the HW method range from 24×10^{-6} at 20 MPa to 37×10^{-6} at 200 MPa. We have compared results of the HW method to the present NIST hydraulic pressure scale. For the entire pressure range, there is agreement in A_e within the combined standard uncertainty ($k = 1$).

1. Introduction

Piston gauges (PGs) are used as primary and secondary pressure standards at national metrology institutes for pressures of 0.1 MPa and above. In the pneumatic region below 1 MPa, large diameter PGs supported with improved dimensional capability and manometric pressure standards make it possible to achieve a relative standard uncertainty in pressure of a few parts in 10^6 [1]. Uncertainties in the hydraulic pressure region can be significantly higher, in particular above 100 MPa. This results from the smaller diameter piston required to keep the mass load to a reasonable limit and from the distortion of the piston and cylinder becoming more significant. A widely used pressure standard above 100 MPa is the controlled clearance piston gauge (CCPG) [2–5]. In a CCPG, a pressure independent of the system pressure is applied to the outside of the cylinder. This 'jacket pressure' minimizes the elastic distortion of the cylinder and controls the annular gap between the piston and cylinder. Heydemann and Welch (HW) [2] describe a method for characterizing a CCPG that involves dimensional measurement of the piston area and estimates of the piston–cylinder gap; the gap is estimated using measurements of fall rate of the piston and changes in system pressure in response to changes in jacket pressure. Using the HW method, a CCPG can be characterized as a primary pressure standard, i.e. without extrapolation from another pressure standard. Presently, the uncertainty in A_e determined by the HW method is higher than the stability and resolution of state-of-the-art hydraulic PGs. This results in large uncertainties in the effective area of secondary standard

PGs that are traceable to the CCPG. We are exploring whether smaller, more compact CCPG designs using small mass loads, reduced axial stresses in the cylinder and computer monitoring of operational parameters can reduce the uncertainties.

Recently, DH Instruments, USA[3] have introduced an oil-operated CCPG that uses a standard 100 kg mass set to generate pressure from 10 MPa to 200 MPa [6]. The CCPG is built on a platform used for a commercially available line of free deformation hydraulic PGs, taking advantage of its fabrication, instrumentation and monitoring methods. This device can operate with jacket pressures up to 100% of the measured pressure or 100 MPa, whichever is less. Modules containing a range of piston cylinder sets can be interchanged in a common column. The CCPG can also be operated in free deformation mode with an estimated pressure deformation coefficient of 7.1×10^{-7} MPa $^{-1}$ at 200 MPa with a load of 100 kg.

The present paper summarizes results on measurements of this CCPG (designated as CCPG-537) using the pressure transmitting fluid di(2-ethylhexyl) sebacate in the pressure range 20 MPa to 200 MPa, along with the HW model to characterize the results. A free deformation type PG (PG479) was cross-floated against CCPG-537 to estimate the measured pressure, p, and the distortion due to changes in the jacket pressure, p_j. The jacket pressure was measured using another PG (PG49). CCPG-537 was cross-floated against another NIST PG, PG21, using Spinesstic fluid to compare the HW model results with the present NIST pressure scale. The measurements were completed two times at NIST, first in 2003 and then again in 2005. Between the two sets of measurements, CCPG-537, along with all the other NIST PG standards, was disassembled and moved from Building 220 at NIST to Building 218 of the Advanced Measurement Laboratory (AML) at NIST.

2. Experimental setup and description of piston and cylinder

The experimental setup is shown in figure 1. A common pressure line supplies hydraulic pressure to both CCPG-537 and PG479. Two constant volume valves (CVV) isolate the PGs from the pressure line and from each other. Manual isolation valves are also connected in line and act as (small volume) high pressure pumps for the minor adjustment of the equilibrium level of the pistons during experimentation. The jacket pressure of CCPG-537 was generated and measured with PG49 as shown. For the calibration of CCPG-537 against PG21, CCPG-537 was moved to the bench containing PG21. The setup was the same as shown in figure 1 with PG21 in place of PG479.

The on-board sensors of the base unit measure the temperature of the piston–cylinder module, the floating position of the piston relative to a reference point, the rotation rate of the piston, relative humidity, ambient pressure and ambient temperature. The piston and masses can be rotated with a motor and belt drive, although we rotated the system manually. The base unit is supported by an interactive terminal

[3] Certain commercial equipment, instruments or materials are identified in this paper to foster understanding. Such identification does not imply endorsement by the NIST nor does it imply that the equipment or materials are necessarily the best available for the purpose.

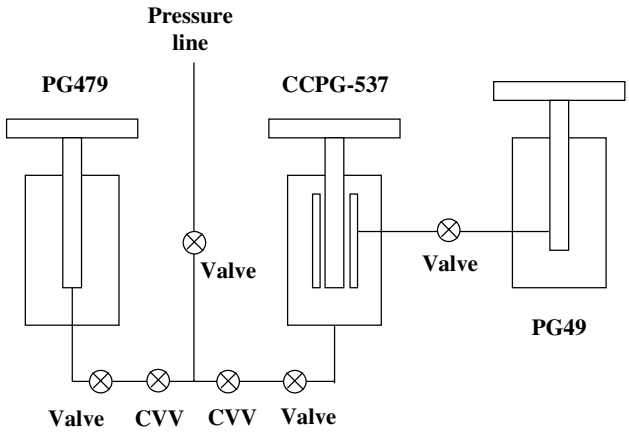

Figure 1. Schematic of experimental apparatus for characterizing CCPG-537.

that can be addressed by common personal computer (PC) communication protocols, and all measured parameters are available for the computer. We monitored and recorded piston position, temperature, rotation rate and ambient conditions. The change in piston position with time, commonly referred to as fall rate, is determined by fitting a linear regression line to the recorded position versus time data of the piston. The piston is operated at midstroke with a nominal rotation rate of 30 revolutions per minute (rpm). During a cross-float experiment between CCPG-537 and either PG479 or PG21, we determine pressure equilibrium by the fall rate method [3]. In this method, the fall rates of the test and reference PGs are determined with the gauges isolated (CVVs closed). The pressure line between the two is opened, and the fall rates are redetermined. If the fall rates change when the valve is opened, mass is adjusted on the reference gauge, and the process is repeated until opening the valve produces no change in fall rate.

The piston and cylinder of CCGP-537 are both made of tungsten carbide. The nominal outer diameter of the piston is 2.5 mm and it is 60 mm long. The length of engagement (narrowest gap) between the piston and cylinder is 30 mm, and it extends from 10 mm above the lower surface of the piston to 20 mm below the top surface. The cylinder is shown in figure 2. The inner diameter over the engagement region is 2.5 mm and the outer diameter is 24 mm. The cylinder is 50 mm long, and the engagement region extends down from the top surface to 30 mm below that surface. The lower 20 mm of the cylinder has an inner diameter of 6 mm and is subjected to the full system pressure in the radial direction. The lower 10 mm of the piston extends into the 6 mm diameter portion of the cylinder at the reference position. All measurements in the present work were done with no more than ± 1 mm vertical movement of the piston from the reference position. Seals are situated on the cylinder such that the entire 50 mm length on the cylinder outer diameter is subjected to the jacket pressure. The jacket pressure loads the cylinder in the axial (vertical) direction over an annular ring from 20 mm diameter to 24 mm on the bottom (upward force) and over an annular ring from 20.5 mm to 24 mm on the top (downward force). The system pressure applies axial upward loading on the chamfer where the inner diameter opens up from 2.5 mm to 6 mm. The net upward axial load from the pressure forces is balanced by a retaining ring on the upper

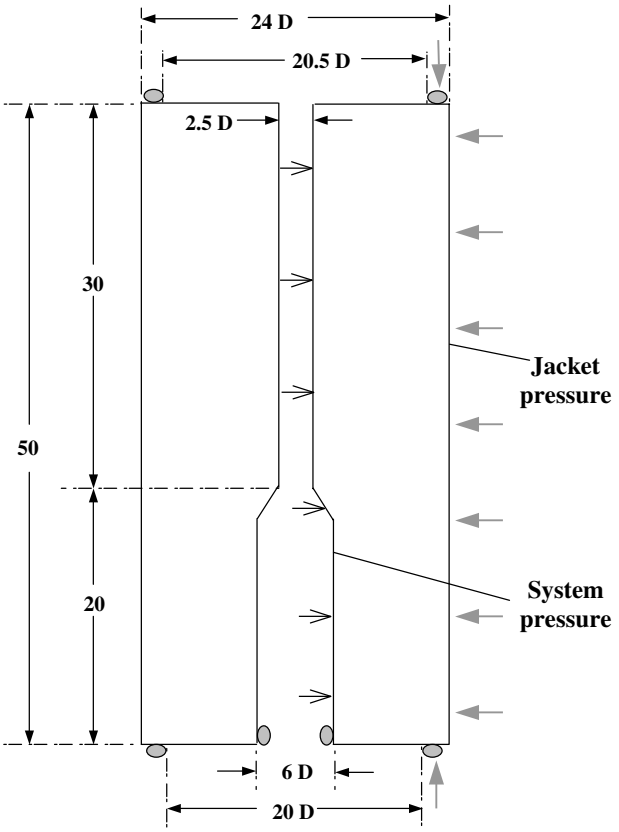

Figure 2. Schematic of CCPG-537 cylinder showing nominal dimensions, pressure loading and seal locations. The engagement region with piston extends from the top surface downward to 30 mm. All dimensions are in millimetres.

cylinder surface acting from a diameter of 6 mm to 20.5 mm. The bottom surface of the cylinder, from the 6 mm diameter to the 20 mm diameter, is subjected to atmospheric pressure.

PG479 and PG49 both operate to 200 MPa full-scale pressure and use 2.5 mm diameter tungsten carbide pistons. PG479 has the same on-board sensors and uses the same PC communication protocols as CCPG-537, and its performance parameters were also monitored and recorded on the computer. The effective area of PG479 has a relative standard uncertainty of 16×10^{-6} and is traceable to the NIST hydraulic pressure scale through a 2005 calibration against PG21 using Spinesstic oil. PG21 is a re-entrant PG with a nominal piston diameter of 3.27 mm, a relative standard uncertainty of 16×10^{-6} and a full-scale operating range of 280 MPa. It is used exclusively with Spinesstic oil.

Two types of characterization experiments were performed on CCPG-537, driven by the requirements of the HW modelling method. Both these sets were completed in 2003 and again in 2005. In the first set of experiments, we measured the fall rate at the common p of 20 MPa, 40 MPa, 60 MPa, 80 MPa, 100 MPa, 120 MPa, 140 MPa, 160 MPa, 180 MPa and 200 MPa for a range of p_j. At each p, fall rate was measured at $p_j = 0$ and then from $p_j/p = 0.1$ to 0.3 in 2003 and $p_j/p = 0.1$ to 0.4 in 2005. The wider range in p_j for 2005 helped assess its effect on the HW model. In the second set of experiments, CCPG-537 was cross-floated against PG479 at the same system pressures (20 MPa to 200 MPa in 20 MPa increments) and the same jacket pressures as for the fall rate experiments. All the above experiments were conducted using di(2-ethylhexyl) sebacate. In 2005, we cross-floated CCPG-537 against PG21 using Spinesstic at the same common system pressures and with $p_j = 0$ only.

3. Characterization of a CCPG using the HW method

Because the HW method is an established and internationally accepted primary method [4,7], we have used it to characterize CCPG-537. Other methods that have been applied to CCPGs include the application of elastic theory with the similarity method [8] and the finite element method (FEM) [9,10]. The data acquired here can be analysed using other methods as well.

The measured pressure at the reference level of a CCPG at equilibrium conditions is determined by using the following equation known as the HW model [2,3]:

$$p = \frac{\sum_i m_i g \left(1 - \frac{\rho_{air}}{\rho_{mi}}\right) + \gamma C}{A_{0p}(1 + bp)\{1 + (\alpha_p + \alpha_c)(T - T_r)\}\{1 + d(p_z - p_j)\}}. \quad (1)$$

Here, m_i is the mass of the weight, ρ_{air} is the density of the air surrounding the masses, ρ_{mi} is the density of the weight, γ is the surface tension of the pressure-transmitting fluid, C is the circumference of the piston where it emerges from the fluid, A_{0p} is the area of the piston at ambient pressure and T_r, α_p and α_c are the thermal expansion coefficients of the piston and cylinder, T is the temperature of the piston–cylinder, T_r is the reference temperature (23 °C), b is the pressure distortion coefficient of the piston, p_j is the jacket pressure applied to the outside of the cylinder, p_z is a HW modelling parameter, equivalent to the jacket pressure for which the clearance between the piston and cylinder is zero at a given measured pressure and d is a HW modelling parameter, equivalent to the relative change of effective area due to a change in jacket pressure.

The numerator in equation (1) represents the mass and surface tension forces on the CCPG, and the denominator is the effective area, A_e:

$$A_e = A_{0p}(1 + bp)\{1 + (\alpha_p + \alpha_c)(T - T_r)\}\{1 + d(p_z - p_j)\}. \quad (2)$$

In the HW model, A_{0p} is determined by dimensional diameter measurements. The piston area at the operating pressure is estimated from the $(1 + bp)$ multiplier on A_{0p}, and analytical distortion formulae are used to estimate b. The change in area due to thermal expansion is estimated by the middle bracket term. The final term in equation (2) approximates the additional area due to the piston–cylinder gap. We imagine applying sufficient jacket pressure to collapse the cylinder onto the piston, reducing the gap to zero and the effective area equal to the piston area only. We then reduce the jacket pressure, opening up the gap and increasing the effective area. p_z is the jacket pressure that reduces the gap to zero, and the amount of area increase per change in p_j is determined by the parameter d. The experimental characterization of a CCPG using the HW model requires determining the parameters p_z and d and their dependence upon the operating conditions, along with a dimensional characterization of the piston. One of the limitations of characterization using the HW model is that operating

the CCPG at jacket pressures close to p_z can potentially damage the piston or cylinder, and the mechanical design of the components must withstand the high jacket pressure.

3.1. Fall rate measurements for determining p_z

Instead of determining p_z by operating the CCPG at a jacket pressure that reduces the gap to zero, the HW model assumes that the gap will change linearly with applied jacket pressure and extrapolates measurements taken at lower pressures. To determine p_z, the HW model utilizes viscous flow theory that predicts that the flow rate (Q) of fluid in the piston–cylinder gap is proportional to the third power of clearance (h) between the cylinder and piston, or

$$Q = h^3 \times \text{const.} \tag{3}$$

The gap flow rate is directly proportional to the fall rate, v, of the piston, assuming no fluid leakage and no thermal expansion of the fluid. The HW model further assumes that the gap width varies linearly with the jacket pressure at each measured pressure, p. The jacket pressure for which the clearance becomes zero, p_z, is computed by measuring v versus p_j (at constant p) and fitting it to the following function:

$$k(v)^{1/3} = p_z - p_j. \tag{4}$$

k and p_z are fitting constants, and p_z is the intercept of the fitted function at $v = 0$. The fall rate measurements are repeated at each of several measured pressures, and a value of p_z is determined for each pressure. p_z values obtained for each p are fitted to a linear function as follows:

$$p_z = p_{z0} + p_{z1} p. \tag{5}$$

p_{z0} can be thought of as the jacket pressure required to close the piston–cylinder gap at zero measured pressure. The fitting parameters can be dependent on the pressure-transmitting medium and therefore are strictly valid only for sebacate [11, 12].

Uncertainty in p_z. The Type A uncertainty[4] in p_z is estimated from the standard uncertainty in the predicted value of the fitting function given by (5) [13]:

$$u_A(p_z) = s \left[\frac{1}{n} + \frac{(p - p_{av})^2}{\sum_{k=1}^{n} (p_k - p_{av})^2} \right]^{1/2}. \tag{6}$$

s is the standard error of the linear fit, n is the number of observations (10 for the 10 pressures), p_k is the measured pressure at the n observations, p_{av} is the mean pressure (110 MPa in the present case) and p is the pressure at which the uncertainty is estimated. A Type B uncertainty was considered based on whether the value of p_z changes if the range of jacket pressure used to determine it changes. The contribution of the Type B uncertainty will be discussed in the results that follow.

3.2. Cross-float measurements for determining d

The HW parameter d is determined by monitoring the change in measured pressure due to the change in jacket pressure at each constant load [3]:

$$d = \frac{1}{p} \frac{\partial p}{\partial p_j}. \tag{7}$$

The definition of d follows from taking the partial derivative of both sides of equation (1) with respect to p_j, holding the load constant and neglecting higher order terms. p is measured by cross-floating CCPG-537 against PG479, at each constant mass load, over the range in jacket pressures. The p versus p_j data are fitted to a linear function, and d is the fitted slope divided by an average value of p. Using an average p is justified since the relative change in pressure produced by changes in p_j is less than 2.4×10^{-4}, and this contributes an error in the relative effective area of less than 0.14×10^{-6} (0.14 ppm). The results for d at each nominal pressure are then fitted to a linear equation:

$$d = d_0 + d_1 p, \tag{8}$$

where d_0 and d_1 are fitting constants. As with p_z, the fitting parameters can be dependent on the pressure-transmitting medium.

Uncertainty in d. The Type A standard uncertainty in d is estimated from the standard deviation of the predicted values of the fitting function, following equation (6). Analytical stress models predict that d is invariant with pressure to first order. Equation (7) shows that with constant d, the change in p due to a unit change in p_j is proportional to p; hence it is more difficult to make the d measurements at low pressure.

3.3. Piston distortion coefficient b

Modelling the piston as uniformly loaded on the ends at p and pressurized in the gap at common pressure $p/2$, the analytical formula to determine the piston distortion coefficient is [2]

$$b = -(1 - 3\mu)/E_p. \tag{9}$$

We use Poisson's ratio, μ, of 0.218 and modulus of elasticity, E_p, of 5.6×10^{11} N m^{-2} provided by the manufacturer, and find $b = -0.617 \times 10^{-6}$ MPa^{-1}. The standard uncertainty in b is taken as $u(b) = 0.03b$.

3.4. Piston area

The piston diameter was measured at the NIST Engineering Metrology Group using a contact micrometer combined with a laser displacement interferometer [14]. Measurements were made in 2.5 mm increments over the 30 mm engagement length (13 locations total) along two angular planes, 0° and 90° from the first plane. The reference temperature for the dimensional measurements was 20 °C. The standard uncertainty in the diameter measurement is 20 nm. Figure 3 shows the data with the standard uncertainty as error bars. The zero vertical location is the midpoint of the piston in the engagement region (25 mm from the bottom surface of the piston). The data show some vertical profile to the piston, with larger diameters near the top. The maximum difference in piston diameter is about 100 nm. The difference in diameter between angular planes is less than the uncertainty of the measurement. An unweighted average of the 26 diametrical measurements gives an area of 4.900 431 mm^2 (20 °C) with a relative standard uncertainty of 16.0×10^{-6}, based entirely on the uncertainty of the measurements.

[4] Unless otherwise stated, all uncertainties stated in this paper are standard uncertainties, i.e. $k = 1$.

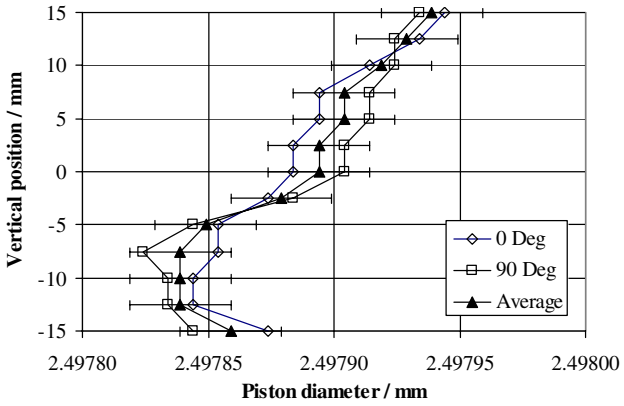

Figure 3. Piston diameters versus vertical position along 30 mm engagement region. Zero position is midway between top and bottom of engagement. The standard uncertainty of dimensional measurement (20 nm) is shown as an error bar on average data.

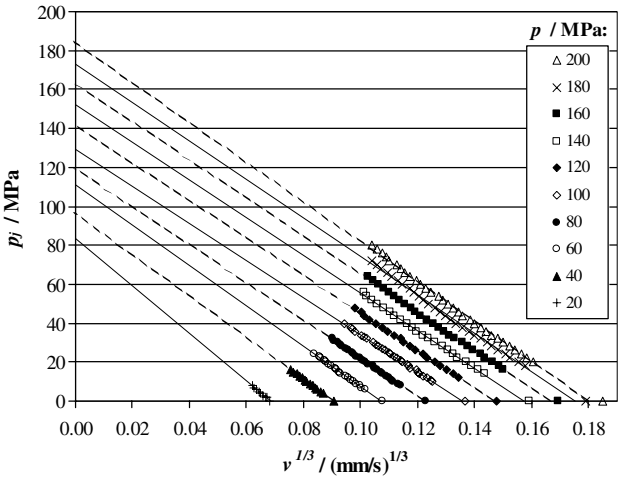

Figure 4. Fall rate (v) of CCPG-537 from 2005 over $p_j/p = 0$ to 0.4, plotted as p_j versus $v^{1/3}$, for constant pressure (p). Linear fits of data over same range are extrapolated to $v = 0$, giving the HW parameter p_z.

The 100 nm variation in piston diameter due to the vertical profile is larger than the dimensional uncertainty. Because of the likely non-linear pressure distribution in the gap resulting from viscosity variations and elastic distortion, the average diameter may not yield the 'effective area' of the piston. We therefore calculate an uncertainty in area due to the profile, by modelling the diameter as a triangular distribution with upper limits and lower limits equal to the largest and smallest dimensional diameter (averaged at each height from the 0° and 90° planes). A triangular distribution is chosen because there is a 100% probability that the diameter lies between the upper and lower limit, and the average diameter is more likely to be correct than the upper and lower limit. The relative standard uncertainty from the profile is 16.3×10^{-6}.

The reference temperature for the effective area is 23 °C. Using a coefficient of thermal expansion for the piston of $4.5 \times 10^{-6}\,\mathrm{K}^{-1}$, we find $A_{0p} = 4.900\,563\,\mathrm{mm}^2$. The uncertainty in the piston area must include the additional uncertainty from raising the reference temperature from 20 °C in the dimensional metrology lab to 23 °C. Assuming a relative standard uncertainty in the piston thermal expansion coefficient of 0.058, this component of uncertainty is 1.57×10^{-6}. The combined relative standard uncertainty in A_{0p} is 22.9×10^{-6} (22.9 ppm).

4. Results of the characterization

4.1. Fall rate measurements to determine p_z

The results of the fall rate measurements for the various jacket pressures and system pressures from the 2005 data are plotted in figure 4. For the 2005 data, p_j/p varied from 0 to 0.4. The cube root of the fall rate ($v^{1/3}$) is plotted on the x-axis, the y-axis shows p_j, and constant system pressures are designated by similar symbols. The 2003 data look very similar to the 2005 data, except that p_j/p extends only up to 0.3. The lines plotted on the figure are the linear regression fits of the data using equation (4) for each system pressure. The intercept of each fitted line and the y-axis is the HW parameter p_z. Visually the data show good linearity, particularly up to $p = 120$ MPa. Close examination of the residuals about the linear regression fits for 140 MPa and above shows curvature, which can be visually seen in the figure for $p = 200$ MPa. For the higher pressures, the x-axis intercepts of the regression lines also deviate from the measured fall rates at $p_j = 0$, another indication of non-linearity in p_j versus $v^{1/3}$.

To make a direct comparison between the 2003 and 2005 measurements, we also fit the 2005 data over the p_j/p range of 0 to 0.3. The results of the 2005 and 2003 determinations of p_z are listed in table 1 and plotted in figure 5. We further fit the 2005 data over the limited p_j/p range of 0.2 to 0.4. Two trends are apparent from the data. First, except for the pressures of 120 MPa and 20 MPa, the agreement between 2003 and 2005 for $p_j/p = 0$ to 0.3 is quite good; the average difference in p_z from 2003 to 2005 was 0.66 MPa, omitting values at 120 MPa and 20 MPa. The high p_z at 120 MPa for 2003 is likely due to temperature stability problems. The environmental temperature on that test date rose by about 1 °C and then fell by 0.5 °C. Due to thermal expansion of the hydraulic fluid, we would expect rising temperatures to underestimate the fall rate and falling temperatures to overestimate the fall rate. These conditions and the order in which the jacket pressure was changed would explain the high value of p_z. Measurements at 20 MPa were the most difficult, due to the very low fall rates at those conditions (the piston drops by 1 mm in an hour at 20 MPa). Excluding these two points, CCPG-537 has repeatable fall rates and p_z values.

The second noticeable trend is that the p_z parameter increases if the range in the jacket pressures used in the linear fits is shifted to higher values. This is a consequence of the curvature in the p_j versus $v^{1/3}$ data discussed above. At 200 MPa, p_z increases by 8.3 MPa if the highest p_j/p is increased from 0.3 to 0.4. A further increase in p_z occurs if data from $p_j/p = 0.2$ to 0.4 are used in the fit. If the non-linearity in the data of figure 4 is viewed in terms of the piston–cylinder gap, it means that the gap is not closing at the same rate with high jacket and system pressure as it is with low jacket and system pressure. We note that a 3 MPa change in p_z will produce about a 10×10^{-6} (10 ppm) relative change in the effective area of the CCPG.

Table 1. HW parameter p_z determined from fall rate measurements of 2003 and 2005. For 2005, p_z is determined from several ranges of p_j/p. Type A, Type B and combined standard uncertainty are shown from 2005 data.

	Estimated p_z/MPa				Uncertainty/MPa, 2005		
	2003	2005			$u_A(p_z)$	$u_B(p_z)$	$u_C(p_z)$
p_j/p	0 to 0.3	0 to 0.3	0 to 0.4	0.2 to 0.4	0 to 0.4	0 to 0.4	0 to 0.4
p/MPa							
20	67.01	79.63	83.71	93.22	0.89	0.92	1.28
40	98.52	98.65	97.18	94.18	0.76	1.84	1.99
60	109.01	109.33	111.18	112.63	0.64	2.76	2.84
80	121.19	118.36	120.07	121.31	0.54	3.68	3.72
100	126.58	128.10	129.60	131.15	0.49	4.60	4.63
120	153.62	139.16	142.17	146.66	0.49	5.53	5.55
140	147.45	148.47	152.42	157.25	0.54	6.45	6.47
160	159.69	157.51	163.43	171.02	0.64	7.37	7.39
180	167.51	165.25	173.25	182.53	0.76	8.29	8.32
200	177.39	176.40	184.68	193.89	0.89	9.21	9.25

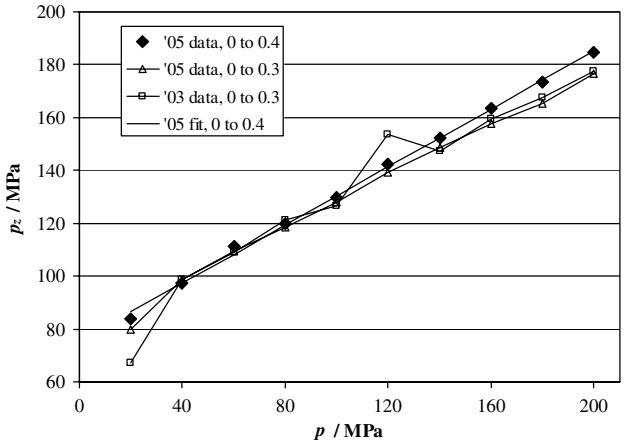

Figure 5. HW parameter p_z as a function of p. Data and fit shown for $p_j/p = 0$ to 0.4, 2005 measurements. Data only shown for $p_j/p = 0$ to 0.3 from 2003 and 2005.

Fitting the 2005 p_z data obtained from $p_j/p = 0$ to 0.4 to a straight line, we get the following equation:

$$p_z = 75.37 + 0.549p, \qquad s = 1.51. \tag{10}$$

The units for p, p_z and s (the standard error of the straight line fit) are MPa. The straight line fit is plotted in figure 5.

Although we could use higher order models or limited ranges of the jacket pressure to estimate p_z from the fall rate data, in the present characterization we are holding to the spirit of the simplicity of the HW model. We do not attempt to adjust the model to match the result from another pressure standard.

4.2. Uncertainty in p_z

The Type A uncertainty in p_z, $u_A(p_z)$, was calculated from equation (6) with s from equation (10) and is listed in table 1. It ranges from 0.49 MPa at (100 and 110) MPa to 0.89 MPa at (20 and 200) MPa. As can be seen from the above results, values of p_z depend on the range of jacket pressures used in its determination. This relates to whether the modelling assumption of extrapolating the p_j versus $v^{1/3}$ data can estimate the zero-gap condition. We include a Type B uncertainty that reflects our uncertainty in the jacket pressure range necessary to estimate p_z.

We estimate this uncertainty using the difference in the p_z values for the 0 to 0.4 range of p_j/p compared with the 0.2 to 0.4 range. We model the possible p_z at $p = 200$ MPa as a normal distribution, with a best estimate of 184.7 MPa and an upper limit of 193.9 MPa. With about a one out of three chance that the true value lies between the upper limit and the best estimate [15], the standard uncertainty due to the model is the difference between the best estimate and the upper limit, or $u_B(p_z) = 9.21$ MPa. We further assume, as indicated by figure 5, that the difference between the best estimate and the upper limit increases linearly as p increases, or

$$u_B(p_z) = 0.0461p. \tag{11}$$

The combined standard uncertainty, $u_C(p_z)$, is the sum in quadrature of the Type A and Type B uncertainties and is listed in table 1. The Type B uncertainty is the largest component in $u_C(p_z)$, which ranges from 1.3 MPa at low pressure to 9.3 MPa at high pressure.

4.3. Cross-float measurements to determine d

The HW d parameter was determined by a cross-float comparison to PG479. Results of the cross-float measurements for the 2005 data are shown in figure 6, where we have plotted A_e (at 23 °C) of CCPG-537 versus p_j along lines of nominally constant p. The range of p_j/p is 0 to 0.4. A_e was determined from the forces on CCPG-537 divided by the pressure measured by PG479. These data could be used directly to characterize the CCPG through PG479, but in that case the gauge would not be a primary standard and would receive its effective area from the existing NIST pressure scale. In the HW model, only the derivative $\partial p/\partial p_j$ is required, so relative uncertainties in p or A_e of the reference PG of order 10^{-4} are sufficient. Effective area data from 2003 over $p_j/p = 0$ to 0.3 agree very well with the 2005 effective area over the same jacket pressure range. At 40 common pressures, the average of the relative differences in A_e between 2003 and 2005 was 1.1×10^{-6} (1.1 ppm). This agreement represents a combined stability of both PG479 and CCPG-537 over the two-year period.

Calculations of d for 2003 and 2005, obtained from fitting the cross-float data to straight lines and taking the slope of the fit, are listed in table 2 and plotted in figure 7. As in the determination of p_z, we computed d for 2005 using two ranges of p_j/p: 0 to 0.3 and 0 to 0.4. There was no evidence of non-linearity in d at the higher jacket pressures. The agreement in d between the two ranges in jacket pressures, defined as the average of the difference in d using the two ranges, is 3.0×10^{-8} MPa^{-1}. This compares with the standard error of a linear fit of d versus p, for $p_j/p = 0$ to 0.4, of 5.9×10^{-8} MPa^{-1}. Hence any change due to the range of jacket pressure is smaller than the random error of the data. The d parameter was also consistent between 2003 and 2005, although the Type A uncertainty was higher in 2003. The d values for 2003 were on average 0.5×10^{-8} MPa^{-1} lower than in 2005. In 2003 the standard error of the linear fit of d versus p was 1.5×10^{-7} MPa^{-1}. Table 2 shows two determinations of d at $p = 100$ MPa for 2003 that agreed with 1.0×10^{-7} MPa^{-1}. We believe the larger uncertainty in 2003 was due to the greater variation in ambient temperature during the cross-float measurements.

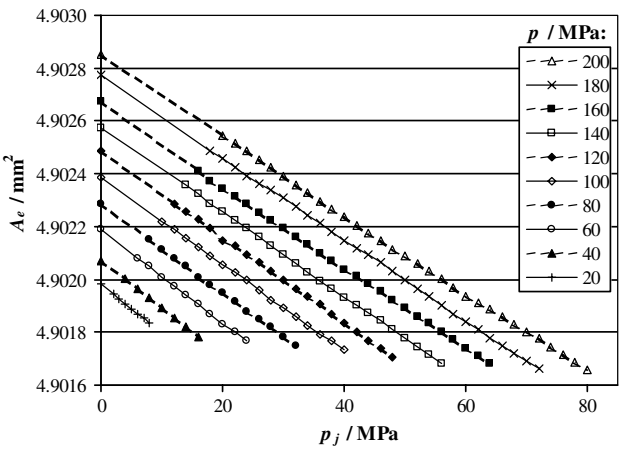

Figure 6. Effective area, A_e, of CCPG-537 from cross-float to PG479, 2005 data. The range of p_j/p is 0 to 0.4. Similar symbols are constant p.

The linear fit of d versus p for the 2005 data over $p_j/p = 0$ to 0.4 yields

$$d = 3.805 \times 10^{-6} - 4.01 \times 10^{-9} p, \qquad s = 5.89 \times 10^{-8}. \tag{12}$$

The fitted line is also shown in figure 7. The units for d and s are MPa^{-1}. The d parameter can also be estimated analytically, assuming the cylinder has no end loading and uniform radial loading at $p/2$ on the inner surface and p_j on the outer surface. The analytical estimate of d is 3.5×10^{-6} MPa^{-1}, which is midway between the extremes of the measured values.

4.4. Uncertainty in d

The Type A uncertainty in d, $u_A(d)$, is estimated from the standard deviation of the predicted value of the fitted line and is listed in table 2 at the nominal measured pressures. The values range from 1.89×10^{-8} MPa^{-1} at (100 and 110) MPa to 3.46×10^{-8} MPa^{-1} at (20 and 200) MPa. There is no measurable dependence of d on the range in p_j/p used in its determination, so we set the combined uncertainty equal to the Type A uncertainty.

4.5. Combined uncertainty in A_e from HW characterization

The uncertainty in the effective area, $u(A_e)$, in the HW characterization of CCPG-537 is found by the methods described in [15] applied to equation (2). Individual component uncertainties, $u(A_{0p})$, $u(b)$, $u(p_z)$ and $u(d)$, have been described above. We evaluate the uncertainty at the reference temperature of 23 °C and therefore ignore uncertainties in T, α_c and α_p. The effect of the uncertainty in p_j on $u(A_e)$ is negligible. When the PG is used to generate pressure or to calibrate the effective area of another PG, uncertainties due to masses, air density, mass density, gravity, temperature and thermal expansion must be included as appropriate.

Table 3 summarizes the relative combined standard uncertainty, $u(A_e)/A_e$, for nominal pressures from 20 MPa to 200 MPa. Two jacket pressure conditions are considered: $p_j = 0$ and $p_j/p = 0.4$. The component and combined uncertainties at $p_j = 0$ are plotted in figure 8. Uncertainties at these

Table 2. HW parameter d from cross-float measurements of 2003 and 2005. For 2005, d is determined from two ranges of p_j/p. Type A standard uncertainty is shown from 2005 data.

	Estimated d/MPa^{-1}			Uncertainty/MPa^{-1}
	2003	2005		2005, $u_A(d)$
p_j/p p/MPa	0 to 0.3	0 to 0.3	0 to 0.4	0 to 0.4
20	3.286×10^{-6}	3.814×10^{-6}	3.761×10^{-6}	3.461×10^{-8}
40	3.609×10^{-6}	3.707×10^{-6}	3.683×10^{-6}	2.935×10^{-8}
60	3.758×10^{-6}	3.615×10^{-6}	3.605×10^{-6}	2.468×10^{-8}
80	3.475×10^{-6}	3.419×10^{-6}	3.383×10^{-6}	2.100×10^{-8}
100	3.445×10^{-6}			
100	3.547×10^{-6}	3.371×10^{-6}	3.344×10^{-6}	1.890×10^{-8}
120	3.432×10^{-6}	3.309×10^{-6}	3.314×10^{-6}	1.890×10^{-8}
140	3.248×10^{-6}	3.300×10^{-6}	3.268×10^{-6}	2.100×10^{-8}
160	3.221×10^{-6}	3.147×10^{-6}	3.100×10^{-6}	2.468×10^{-8}
180	3.186×10^{-6}	3.140×10^{-6}	3.146×10^{-6}	2.935×10^{-8}
200	3.042×10^{-6}	3.109×10^{-6}	3.031×10^{-6}	3.461×10^{-8}

two jacket pressure conditions bound the uncertainties at intermediate jacket pressures. Over the range of conditions tested, $u(A_e)/A_e$ varies from 23.6×10^{-6} (23.6 ppm) at 20 MPa to 36.8×10^{-6} (36.8 ppm) at 200 MPa. The uncertainty in the piston area contributes a constant relative amount of 22.9×10^{-6} (22.9 ppm). The largest relative uncertainty from a HW parameter is $u(p_z)d$, which is pressure dependent and varies from 4.8×10^{-6} at 20 MPa to 27.8×10^{-6} at 200 MPa. The Type B component of $u(p_z)$, resulting from the modelling assumption of finding the zero gap condition from the fall rate data, is much larger than the Type A uncertainty from the fit of p_z. The relative contribution of $u(d)$ can be reduced by operating at higher jacket pressure, but this effect on $u(A_e)/A_e$ is small.

An approximate equation that can be used to calculate the relative uncertainty throughout the parameter range, with p and p_j in MPa, is

$$u(A_e)/A_e = \left[(23.85 \times 10^{-6})^2 + (1.42 \times 10^{-7}\,\mathrm{MPa}^{-1} \times p)^2 - (5.49 \times 10^{-8}\,\mathrm{MPa}^{-1} \times p_j)^2 \right]^{0.5}. \quad (13)$$

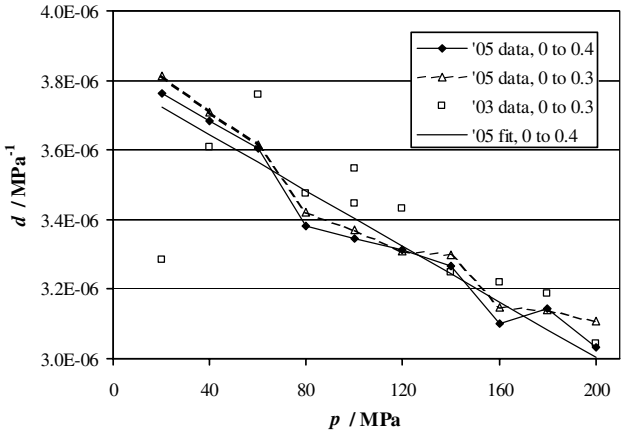

Figure 7. HW parameter d as a function of p. Data and fit are shown for $p_j/p = 0$ to 0.4, 2005 measurements. Data are shown only for $p_j/p = 0$ to 0.3 from 2003 and 2005.

5. Comparison of HW characterization to present NIST pressure scale

The results of the HW characterization of CCPG-537 at zero jacket pressure are compared with the present NIST pressure scale in figure 9. We have plotted the HW model result for A_e versus p along with the cross-float data of CCPG-537 against PG21 and against PG479, both of which are traceable to the present NIST pressure scale. The PG479 path uses the 2005 data taken during the measurement of d. The standard uncertainty in A_e from the HW model is plotted as an error bar. The relative standard uncertainty in A_e from the cross-floats was 17.0×10^{-6} (17 ppm). Figure 10 shows the agreement between the HW model and the two cross-floats as a difference in area, $(A_e^{HW}/A_e^{NIST} - 1)$, with the combined standard uncertainty of the difference plotted as an error bar. As can be seen, there is agreement within the standard uncertainty for all pressures with both the PG21 and PG479 traceability paths. The maximum relative difference was 22.4×10^{-6} for PG21 and 33.3×10^{-6} for PG479. Although there is good agreement between the HW model and the NIST scale, the HW model predicts a non-linear increase in A_e with pressure. Both direct cross-floats showed linear increase with pressure.

The HW model results are compared with the NIST pressure scale at non-zero jacket pressure on CCPG-537 in

Table 3. Relative standard uncertainties in the HW model for component contributions and combined $u(A_e)$. Uncertainties are shown for $p_j/p = 0$ and 0.4.

		Component relative uncertainties × 10^6				Combined × 10^6
p/MPa	p_j/MPa	$u(A_{0p})/A_e$	$u(b)p$	$u(d)(p_z - p_j)$	$u(p_z)d$	$u(A_e)/A_e$
(a) $p_j/p = 0$						
20	0	22.92	0.37	2.99	4.77	23.60
40	0	22.92	0.73	2.86	7.26	24.22
60	0	22.92	1.10	2.67	10.10	25.21
80	0	22.92	1.46	2.51	12.97	26.49
100	0	22.92	1.83	2.46	15.76	27.98
120	0	22.92	2.20	2.67	18.43	29.61
140	0	22.92	2.56	3.20	20.98	31.34
160	0	22.92	2.93	4.03	23.39	33.12
180	0	22.92	3.29	5.11	25.66	34.93
200	0	22.92	3.66	6.41	27.78	36.76
(b) $p_j/p = 0.4$						
20	8	22.92	0.37	2.71	4.77	23.57
40	16	22.92	0.73	2.39	7.26	24.17
60	24	22.92	1.10	2.08	10.10	25.15
80	32	22.92	1.46	1.83	12.97	26.44
100	40	22.92	1.83	1.71	15.76	27.92
120	48	22.92	2.20	1.76	18.43	29.55
140	56	22.92	2.56	2.02	20.98	31.24
160	64	22.92	2.93	2.45	23.39	32.97
180	72	22.92	3.29	3.00	25.66	34.69
200	80	22.92	3.66	3.64	27.78	36.38

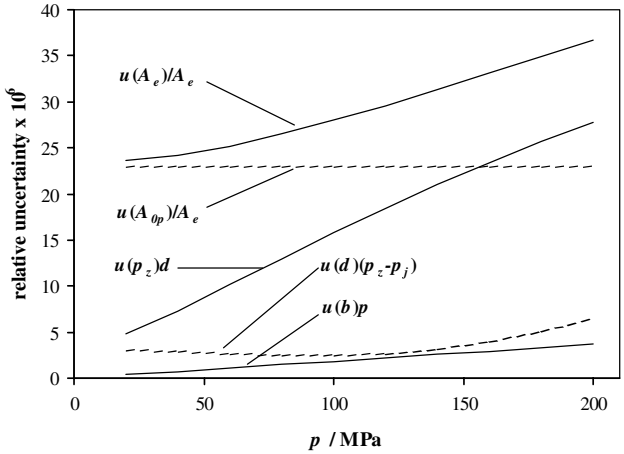

Figure 8. Component and combined relative uncertainties in effective area for the HW model of CCPG-537 at $p_j = 0$.

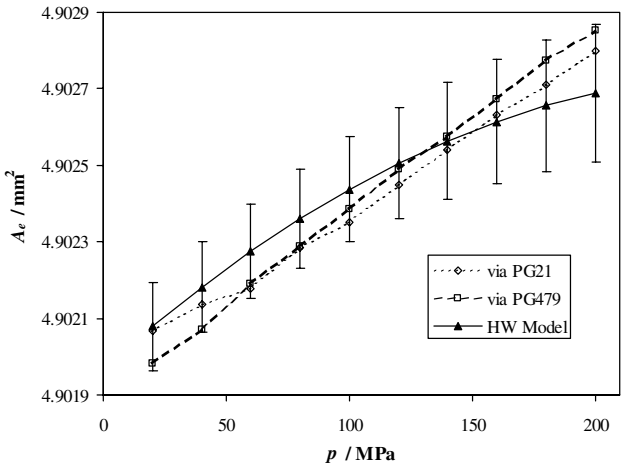

Figure 9. A_e versus p for CCPG-537 at $p_j = 0$ from the HW model and from calibration to the NIST pressure scale via PG21 and PG479. The standard uncertainty from the HW model is shown as error bars.

figure 11. Here, we plot A_e versus p along lines of constant p_j/p (0.1, 0.2, 0.3 and 0.4). The direct link to the NIST pressure scale comes from the cross-float to PG479, which was also used in determining the d parameter. The plots show how increasing the jacket pressure reduces the distortion and that under certain conditions the CCPG can be operated at approximately constant A_e as p is increased. The difference between the HW model and the NIST pressure scale is dependent on system pressure but not jacket pressure. For all p_j/p, A_e predicted by the HW model is about 22×10^{-6} higher at 40 MPa, and 33×10^{-6} lower at 200 MPa, than the NIST scale. All jacket pressures show a similar non-linearity of A_e with p.

6. Discussion of results

Characterization of CCPG-537 using the HW model shows agreement with the present NIST pressure scale to within the combined standard uncertainty, and the method does not require direct traceability to another pressure standard to obtain the characterization. The model predicts non-linear distortion

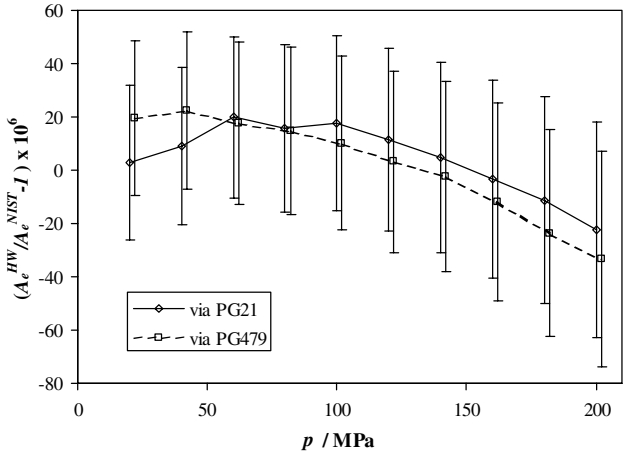

Figure 10. Agreement in effective area of CCPG-537 from the HW model (A_e^{HW}) and direct comparison to the NIST pressure scale (A_e^{NIST}) via PG21 and PG479 at $p_j = 0$. The difference is positive when A_e from the HW model is higher than that from the NIST pressure scale. The combined standard uncertainty of the area difference is shown as error bars.

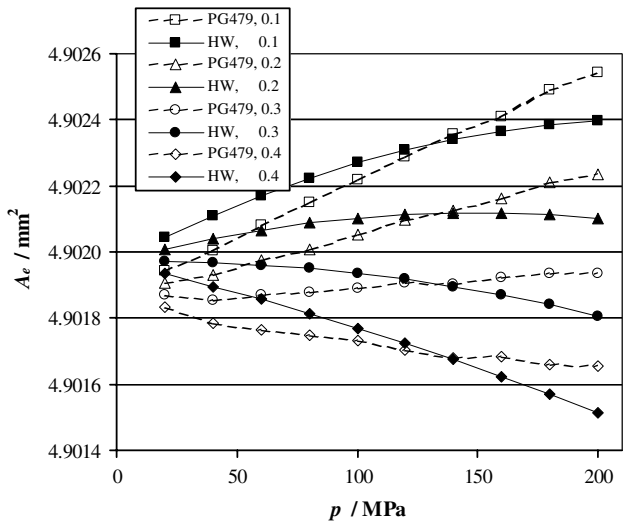

Figure 11. A_e versus p for CCPG-537 at $p_j/p = 0.1$, 0.2, 0.3 and 0.4 from the HW model and from calibration to the NIST pressure scale via PG479.

for conditions of constant p_j/p, including $p_j = 0$. The non-linearity is likely a result of the method for estimating the HW parameter p_z that uses measurements far from the condition where the piston–cylinder gap is zero. At $p = 200$ MPa the model predicts that p_j of 185 MPa will close the gap; however, the design is limited to 100 MPa (and we operated to 80 MPa). The non-linearity in the fall rate curves (figure 4) indicates that using higher jacket pressures will extrapolate to higher p_z, particularly for the higher operating pressures. Larger p_z at higher pressures would likely improve the linearity of A_e predicted by the HW model.

If p_z could be determined from higher jacket pressure measurements, the HW model then requires determining the change in area as the jacket pressure is reduced from p_z to the operating condition. Hence, d would need to be determined over a much wider range of jacket pressure as well.

Measurements of d for p_j/p up to 0.4 do not indicate any dependence on p_j.

A possible alternative to the HW model would be to use the fall rate data in a more quantitative way to estimate the piston–cylinder gap, rather than as an estimation of the jacket pressure required to close the gap. The viscous solution of fluid flow through parallel plates, along with the viscosity versus pressure dependence of the hydraulic fluid, could be solved at conditions of the measured fall rates to determine the radial gap. The cross-float measurements, which provide changes in area with jacket pressure, could be incorporated into the analysis. We note, however, that determining the gap from the fall rate requires an assumption of how the axis of the piston aligns with the axis of the cylinder; in essence, whether there is a uniform gap around the circumference of the piston. It can be shown that the fall rate for a given average piston–cylinder gap can increase by a factor of 2.5 as the piston is moved from the centred location to just touching the cylinder surface. Similarly, non-uniform gaps around the circumference due to an out-of-round piston or cylinder will result in fall rates larger than predicted by an average radial clearance. Hence, any departure from a uniform gap will result in overestimations of the gap from the fall rate data.

7. Conclusion

We have carried out a complete characterization of CCPG-537 two years apart at the NIST using the HW method. The repeatability in relative effective area is 1.1×10^{-6} over the two years. The HW parameters determined from the characterization have also been repeated to within the Type A uncertainty from the two characterizations. The p_z parameter needs to be determined by as high a jacket pressure as possible; because the more recent characterization was performed with a higher jacket pressure, the HW model result is presented using only those data. The relative combined standard uncertainty of the effective area using the HW model ranges from 23.6×10^{-6} at 20 MPa to 36.8×10^{-6} at 200 MPa. Operating at a jacket pressure up to 40% of the system pressure reduces the uncertainty slightly. A parametric model is presented to calculate uncertainty at all conditions of p and p_j. The effective area from the HW model agrees to within the combined standard uncertainty of a direct comparison to the NIST pressure scale at all conditions from 20 MPa to 200 MPa. The A_e and $u(A_e)$ from the HW model at $T_r = 23\,^{\circ}\mathrm{C}$ are given by

$$A_e = A_{0p}(1 + bp)\{1 + (\alpha_p + \alpha_c)(T - T_r)\}\{1 + d(p_z - p_j)\}, \tag{14a}$$

$$u(A_e)/A_e = \left[(23.85 \times 10^{-6})^2 + (1.42 \times 10^{-7}\,\mathrm{MPa}^{-1} \times p)^2 - (5.49 \times 10^{-8}\,\mathrm{MPa}^{-1} \times p_j)^2\right]^{0.5}, \tag{14b}$$

with

$$A_{0p} = 4.900\,563\,\mathrm{mm}^2,$$

$$\alpha_p + \alpha_c = 9.0 \times 10^{-6}\,\mathrm{K}^{-1},$$

$$b = -0.617 \times 10^{-6}\,\mathrm{MPa}^{-1},$$

$$d = 3.805 \times 10^{-6} - 4.01 \times 10^{-9}\,p\ (\mathrm{MPa}^{-1}) \text{ and}$$

$$p_z = 75.37 + 0.549\,p\ (\mathrm{MPa}).$$

Acknowledgments

The authors would like to acknowledge the assistance of Patrick Abbott, Dana Defibaugh, R Gregory Driver, Will Guthrie and Jay Hendricks of NIST, during the investigation. One of the authors (AKB) thanks the Director, National Physical Laboratory, New Delhi, India, for his encouragement and help.

References

[1] Schmidt J W, Jain K, Miiller A P, Bowers W J and Olson D A 2006 Primary pressure standards based on dimensionally characterized piston/cylinder assemblies *Metrologia* **43** 53–9

[2] Heydemann P L M and Welch W E 1975 Piston gauges *Experimental Thermodynamics* vol 2, ed B Leneindre and B Voder (London: Butterworths) pp 147–201

[3] Bean V E 1994 NIST pressure calibration service *NIST Special Publication* 250-39, US Department of Commerce Technology Administration, National Institute of Standards and Technology, USA

[4] Olson D A 2001 Capabilities and uncertainties of the piston gage pressure standard at NIST *Advances in High Pressure Science and Technology* ed A K Bandyopadhyay *et al* (New Delhi, India: National Physical Laboratory) pp 21–6

[5] Newhall D H, Ogawa I and Zilberstein V 1979 Recent studies of float and stall curves in controlled-clearance deadweight testers with a simple piston *Rev. Sci. Instrum.* **50** 964–8

[6] Delajoud P and Girard M 2001 A new oil operated controlled clearance piston gauge for operation to 200 MPa *Advances in High Pressure Science and Technology* ed A K Bandyopadhyay *et al* (New Delhi, India: National Physical Laboratory) pp 33–7

[7] Bandyopadhyay A K and Gupta A C 1999 Realization of a national practical pressure scale for pressures up to 500 MPa *Metrologia* **36** 681–8

[8] Dadson R S, Greig R G P and Horner A 1965 Developments in the accurate measurement of high pressures *Metrologia* **1** 55–67

[9] Molinar G F, Maghenzani R, Cresto P C and Bianchi L 1992 Elastic distortions in piston–cylinder units at pressures up to 0.5 GPa *Metrologia* **29** 425–40

[10] Sabuga W 1995 Elastic distortion calculations at PTB on LNE 200 MPa pressure balances as part of EUROMET project 256 *PTB-W-63, PTB (Braunschweig)*

[11] Sharma J K N and Bandyopadhyay A K 1991 Effect of viscosity of the pressure transmitting fluid on the metrological characterization of the piston gauge up to 1 GPa *Pramana—J. Phys.* **37** 363–71

[12] Bandyopadhyay A K, Hilsch P and Jaeger J 1987 Use of controlled-clearance high pressure balances with highly viscous pressure transmitting media *PTB-Mitt.* **97** 264

[13] Engineering Statistics *NIST/SEMATECH e-Handbook of Statistical Methods* http://www.itl.nist.gov/div898/handbook/
Guthrie W 2005 private communication, NIST, USA

[14] NIST Engineering Metrology Group 2004 *Report of Calibration, NIST Test. No.* 821/256581-03

[15] Taylor B N and Kuyatt C E 1994 Guidelines for evaluating and expressing the uncertainty of NIST measurement results *NIST TN* 1297